Nanoflare Heating of an X-ray Bright Point Observed by MaGIXS

Biswajit Mondal[1], P. S. Athiray[3,2], Amy R. Winebarger[2], Sabrina L. Savage[2], Ken Kobayashi[2], Stephen Bradshaw[4], Will Barnes[5], Patrick R. Champey[2], Peter Cheimets[3], Jaroslav Dudík[6], Leon Golub[7], Helen Mason[8], David E. McKenzie[2], Christopher S. Moore[7], Chad Madsen[7], Katharine K. Reeves[7], Paola Testa[7], Genevieve D[2]. Vigil, Harry P. Warren[9], Robert W. Walsh[10], Giulio Del Zanna[8]

[1]NASA Postdoctoral Program Fellow at Marshall Space Flight Center, [2]NASA Marshall Space Flight Center, [3]The University of Alabama in Huntsville, [4]Rice University, [5]American University, [6]Czech Academy of Sciences, [7]Smithsonian Astrophysical Observatory, [8]University of Cambridge, [9]Naval Research Laboratory, [10]University of Central Lancashire.

Summary

Nanoflares, potential candidates for solar coronal heating, are challenging to detect directly. However, their existence and properties can be deduced by comparing simulated plasma emissions from nanoflare heating with observations. Our study simulates X-ray Bright Point (XBP) emissions observed by the MaGIXS (Marshall Grazing Incidence X-ray Spectrometer), in conjunction with data from SDO/AIA and Hinode/XRT. Using the field-aligned HYDrodynamics and RADiation (HYDRAD) Code, we model XBP loop emissions and compare them with observations. Loop characteristics are derived from extrapolation of HMI/SDO's observed magnetogram. We assume random nanoflares heat each loop, determined by its length and magnetic field strength. Results indicate frequent occurrences of nanoflares at intervals of every 400s-800s. Additionally, we demonstrate the high sensitivity of MaGIXS and XRT in diagnosing the heating frequency using this method, while AIA passbands are found to be the least sensitive.

Observations

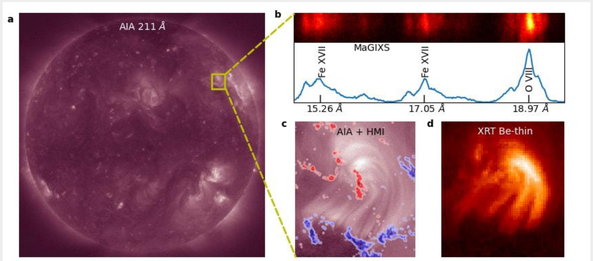

Fig 1. (a) Yellow box denotes the XBP region in the full-Sun image from the AIA 211Å channel on July 30, 2021, at 18:20 UT. (b) MaGIXS captures the spectral and spatial overlapogram of the XBP. (c) A zoomed-in view of the XBP in the AIA 211Å channel with red and blue contours indicating positive and negative polarities in the HMI photospheric magnetogram. (d) XRT's X-ray image of the XBP.

Methodology

1. Magnetic field model of the XBP loops: Utilized potential-field extrapolation from the observed HMI line-of-sight (LOS) magnetogram.

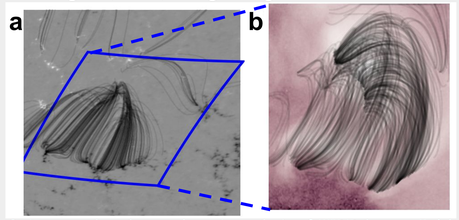

Fig 2. Extrapolated top view (panel a) of XBP loops. Initially, the observed magnetogram was centered along the XBP before extrapolation. Subsequently, these loops were re-projected to align with the Sun-Earth line of sight (LOS) to match AIA observations in panel b.

2. Heating profile: Each loop is heated by random impulsive events according to Parker nanoflare model. The magnitude and the time between two nanoflare events are determined by the loop lengths and magnetic field strength, along with the parker angle (θ) and the horizontal velocity of photospheric driver (V_h).

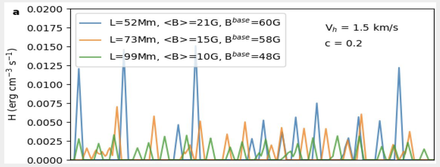

Fig 3. Heating profile for three loops.

3. HYDRAD runs: We use HYDRAD to derive temperature and density variations for each loop based on the heating profile. Establishing this profile involves two unknown parameters, V_h and θ. We assume a range for these parameters and rerun HYDRAD accordingly.

4. Synthetic images: We create synthetic images for each instrument passband by convolving the HYDRAD-obtained DEM with the instrument response function. These synthetic images are then compared with observations.

Results

The synthetic images from HYDRAD simulations, linked to specific heating profiles with V_h and θ values, are compared with observed intensities. Fig 4 showcase a comparison for Vh = 1.5 Km/s and θ = 11° across AIA, XRT, and MaGIXS passbands.

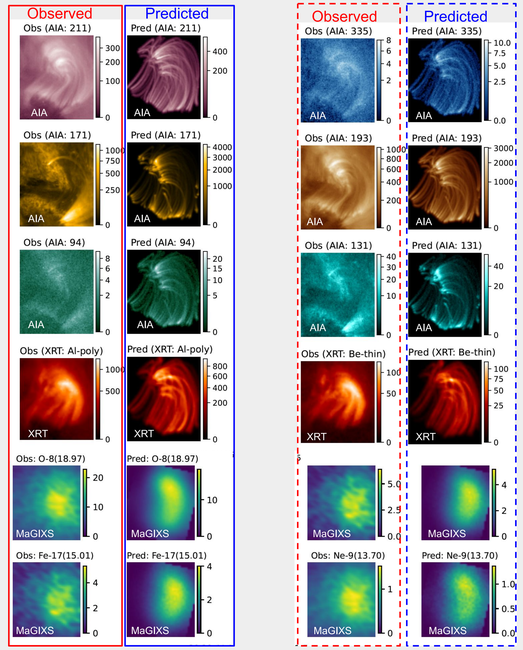

Fig 4. Comparing observed and synthetic images across AIA, XRT, and MaGIXS passbands for Vh = 1.5 Km/s and θ = 11°.

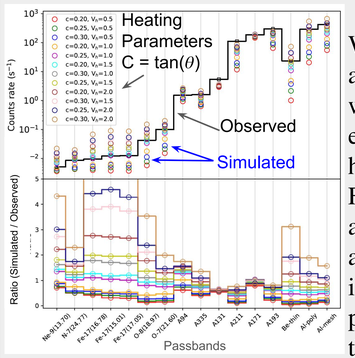

Fig 5. Comparison of average emissions.

We compared observed average XBP emission with synthetic emissions for various heating parameters in Fig 5. Consistent ratios across all passbands for a few simulation runs indicate suitable parameters explaining the observations.

Discussions

The loop-like structures in AIA images closely matched observed emissions overall (Fig 4), except for a distinct bright cool (~1MK) structures, e.g., in 171A (bottom right) passband.

Fig 6 quantifies the agreement between observed and simulated emissions across different heating parameters by examining the deviations (σ) of intensity ratios between observed and simulated emission for all the instrument paasbands.

Converging σ for the heating parameters about V_h = 1.0-1.5 Km/s and θ = 11°-16° (shaded gay region in Fig 6) in both MaGIXS and XRT, indicating a close match with observations.

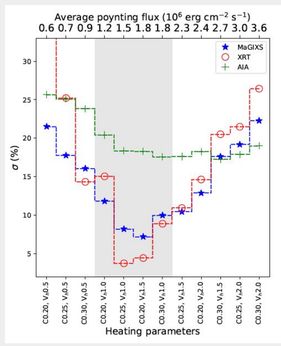

Fig 6. Intensity ratio deviations in observation vs. simulation across all heating parameters.

The shaded area in Fig 6 reflects nanoflare delay times of 400s-800s, significantly shorter than the loops' cooling time (around 10^3s), suggesting high-frequency nanoflares sustain heating in this XBP.

The Poynting flux ranges between 1.0-2.0 $\times 10^6$ erg $cm^{-2}s^{-1}$, intermediate to quiet Sun and active regions.

In Fig 6, the converging trend reveals that XRT and MaGIXS passbands are more sensitive to diagnose average nanoflare heating frequency, while AIA exhibits the least sensitivity in this method.

References

Acknowledgement

Email: biswajit.mondal@nasa.gov